X-parameter based design and simulation of Josephson traveling-wave parametric amplifiers for quantum computing applications

Kaidong Peng
Department of Electrical Engineering and Computer Science
Massachusetts Institute of Technology
Cambridge, United States
kdpeng@mit.edu

Rick Poore
PathWave Software and Solutions
Keysight Technologies, Inc.
Calabasas, United States
rick_poore@keysight.com

Philip Krantz
Quantum Engineering Solutions
Keysight Technologies Sweden AB
Gothenburg, Sweden
philip.krantz@keysight.com

David E. Root
Keysight Laboratories
Keysight Technologies, Inc.
Santa Rosa, United States
david_root@keysight.com

Kevin P. O'Brien
Department of Electrical Engineering and Computer Science
Massachusetts Institute of Technology
Cambridge, United States
kpobrien@mit.edu

Abstract—We present an efficient, accurate, and comprehensive analysis framework for generic, multi-port nonlinear parametric circuits, in the presence of dissipation from lossy circuit components, based on "quantum-adapted" X-parameters. We apply this method to Josephson traveling-wave parametric amplifiers (JTWPAs) – a key component in superconducting and spin qubit quantum computing architectures – which are challenging to model accurately due to their thousands of linear and nonlinear circuit components. X-parameters are generated from a harmonic balance solution of the classical nonlinear circuit and then mapped to the field ladder operator basis, so that the energy associated with each of the multiple interacting modes corresponds to photon occupancy, rather than classical power waves. Explicit relations for the quantum efficiency of a generic, multi-port, multi-frequency parametric circuit are presented and evaluated for two distinct JTWPA designs. The gain and quantum efficiency are consistent with those obtained from Fourier analysis of time-domain solutions, but with enhanced accuracy, speed, and the ability to include real-world impairments, statistical variations, parasitic effects, and impedance mismatches (in- and out-of-band) seamlessly. The unified flow is implemented in Keysight's PathWave Advanced Design System (ADS) and independently in an open-source simulation code, JosephsonCircuits.jl, from the MIT authors.

Index Terms—quantum-limited amplifiers, Josephson traveling-wave parametric amplifier (JTWPA), cryogenic parametric amplifiers, parametric devices, X-parameters, harmonic balance, qubit readout, quantum-mechanical loss model.

I. INTRODUCTION

Nonlinear systems have abundant applications in both classical and quantum settings, ranging from frequency converters and mixers in classical circuits [1] to quantum-limited amplifiers [2], [3] and transducers for quantum computing applications [4]. One of the fundamental cornerstones of building large-scale quantum information processors is access to high-fidelity and scalable qubit readout [5]. The intrinsically low-power operation and frequency-domain multiplexed architecture of dispersive readout – commonly used to readout *e.g.* superconducting [6], [7] and spin qubits [8]–[10] – lays out requirements on signal-to-noise ratio, frequency bandwidth, as well as saturation power of the amplifier chain. To this end, the past decade has seen a rapid development of parametric amplifier technology used to pre-amplify the few-photon level (*e.g.*-150 dBm) readout signals used to probe readout resonators operating at 10 mK to determine the qubit states [11]. Josephson parametric amplifiers (JPAs) [2], [12]–[14] and traveling-wave parametric amplifiers utilizing either nonlinear kinetic inductance [15]–[17] or Josephson nonlinearity [3], [18]–[22] have achieved near-quantum limited noise performance and are now routinely used in superconducting circuit experiments and quantum sensing. JPAs have near-ideal intrinsic quantum efficiency and often consist of one or a few nonlinear resonators. They are compact in footprint and have well-understood behavior [23], [24]. Through impedance and nonlinearity engineering, their bandwidth [25], [26] and dynamic range [27]–[29] can be improved.

Josephson traveling wave parametric amplifiers (JTWPAs) are attractive components given their broad bandwidth (e.g. 3 GHz), high gain (20 dB), high saturation power (-100 dBm), and noise performance approaching the fundamental limit allowed by quantum mechanics [3], [18], [20], [22]. However, despite the suitable characteristics for qubit readout applications, JTWPAs typically consist of thousands of Josephson junctions and thus exhibit more complicated dynamics than JPAs. The design and simulation of JTWPAs with desired performance still constitute a practical bottleneck for many quantum engineers. While simple, analytical two-mode wave-equation models [18], [30]–[32] are commonly used

for device design and modeling, they fall short in predicting realistic multi-mode gain dynamics [33] and quantum efficiency [3], [22] and in capturing non-ideal behaviors observed in experiments, such as the cutoff frequency and photonic bandgaps that originate from the lumped-element nature of the JTWPA design [20], as well as parameter variability associated with fabrication uncertainties [34]–[37]. A harmonic balance method analysis of the signal gain in kinetic inductance traveling-wave parametric amplifiers was performed in [38]; however, for quantum efficiency calculations, the full X-parameter sensitivity matrix must be calculated including for inputs at all of the idler frequencies generated in the parametric processes.

In this work, we present an efficient and accurate circuit-level framework for analyzing the quantum statistics of generic multi-port parametric quantum circuits. This framework is directly applicable to current-pumped JTWPAs exemplified here and is embedded into both the X-parameter analysis flow of Keysight's Pathwave Advanced Design System (ADS) and independently in an open-source simulation code, Josephson-Circuits.jl [39], from the MIT authors. To the best of author's knowledge, this work presents the first quantum efficiency calculation of a circuit quantum electrodynamics parametric device, including loss, using a commercial circuit simulator. The analysis framework is applicable to all harmonic balance solvers. In addition, the unified design, simulation, and analysis flow based on X-parameters can also be applied to model applications requiring multiple pump tone excitations, such as the generation of broadband squeezed vacuum as quantum resource [40], and can be used to integrate multiple nonlinear components and model the overall system measurement efficiency of a qubit readout chain.

Fig. 1(a) shows a diagram of a typical readout-signal path passed through a quantum processor unit (QPU). The signal is then amplified using a JTWPA at the output of the quantum processor at the 10 mK-stage of a cryostat, before the signal reaches the high-electron mobility transistor (HEMT) amplifier at the 4 K-stage and eventually is down-converted and digitally processed using classical room-temperature electronics.

We model the JTWPA as a two-port traveling wave amplifier that converts energy from a large pump tone at angular frequency ω_P to a much smaller in power signal at a frequency ω_s, see Fig. 1(a), which is then amplified. The nonlinearity required for parametric amplification originates from the Josephson junctions (symbols marked with orange "x" in boxes in Fig. 1(b)). Josephson junctions operate based on quantum tunneling of Cooper-pairs through thin barriers, and in this context can be treated as lossless nonlinear inductors. Lack of dissipation is critical for low added noise and to avoid heating the milli-Kelvin environment needed for high-fidelity qubit operation. As the pump and its harmonics interact with the signal, many intermodulation terms are created and propagate further along the structure. Typical input and output spectra are shown in Fig. 2.

Design challenges for JTWPAs include engineering the circuit parameters to simultaneously achieve high gain, broad
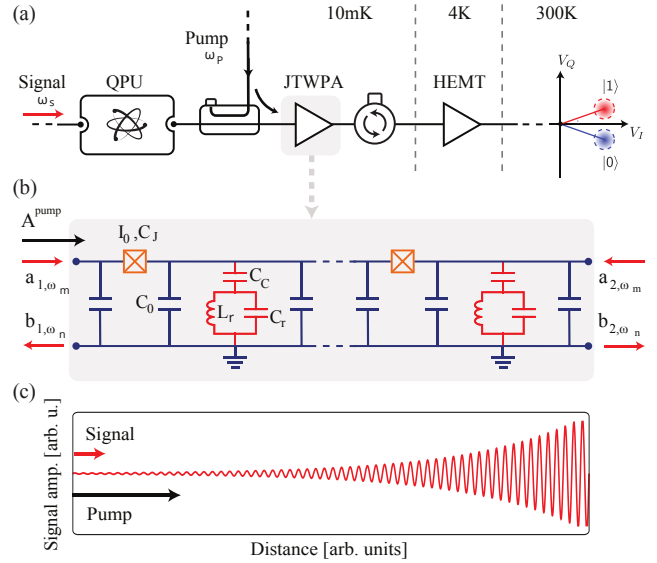

Fig. 1. (a) Simplified schematic of the readout circuitry for a quantum processor (QPU) probed by a weak signal that gets amplified by a JTWPA. (b) Circuit schematic of JTWPA as a lumped-element transmission line built up from unit cells of Josephson junctions (orange boxes), shunt capacitors, as well as phase-matching resonators (red). Note that a realistic device has several Josephson junctions between each phase-matching resonator and dielectric losses which can be accounted for in simulations using a complex capacitance. (c) Cartoon of amplified signal along the length of the JTWPA.

bandwidth, and high quantum efficiency in the presence of realistic fabrication constraints. The parametric amplification process must be phase matched by engineering the nonlinearity or the dispersion by, e.g. creating a stopband around the pump frequency using phase-matching resonators [3], [18], [19] (see red subcircuits in Fig. 1(b)) or through periodic loading [20]. A noteworthy recent development has been the "Floquet" design, whose junction critical current is spatially varied to realize an effective Gaussian nonlinearity profile along the structure. Consequently, the Floquet JTWPA is able to coherently recover information that would otherwise be lost to other sideband modes by adiabatically mode-matching the collective Floquet modes of the nonlinear system to the single frequency modes of the input and output ports, resulting in a quantum efficiency approaching the ideal limit [22]. The designs of the Floquet-mode JTWPA in [22] and the widely used uniform JTWPA in [3] are analyzed using the new methods presented in this work. Their circuit parameters are summarized in Table I. Manufacturing tolerances and other real-world impairments create additional challenges, requiring robust, practical, and flexible modeling and design capabilities to realize optimal performance as part of the quantum computer readout chain.

II. CLASSICAL AND QUANTUM X-PARAMETER FORMULATIONS OF JTWPA

A. Classical X-parameters

Analytical two-mode continuous models [18], [30]–[32] consider only the small signal injected at frequency ω_s and the "image frequency" or primary *idler* at frequency $-2\omega_P + \omega_s$.

TABLE I

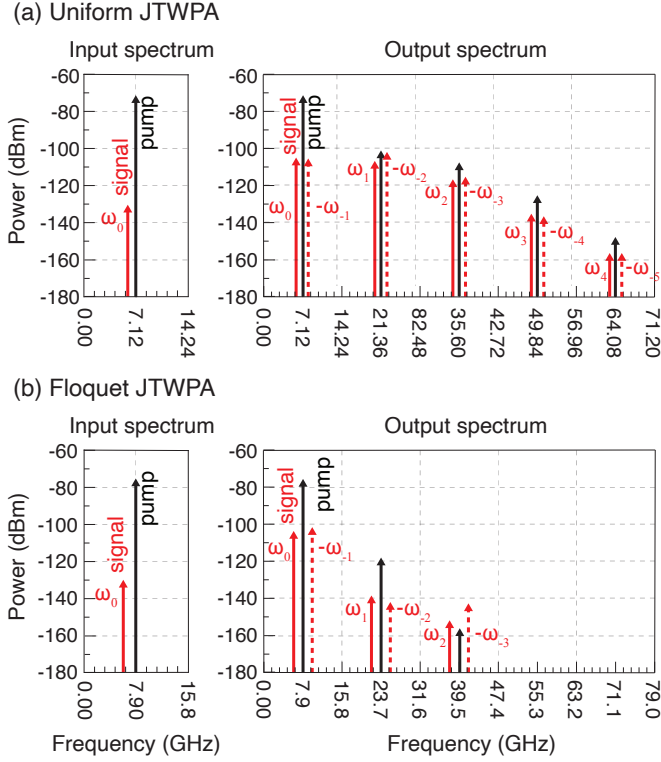| Design	JJ Count	$\omega_P/2\pi$ (GHz)	I_P (μA)	P_P (dBm)	JJ I_c (μA)
Uniform	2047	7.12	3.70	-70.68	3.4
Floquet	3998	7.90	4.40	-69.17	3.50-21.21

Fig. 2. Single-sided input and output spectra for (a) a uniform JTWPA and (b) a Floquet JTWPA respectively, including the pumps and their harmonics. Frequencies are defined according to (1). Negative frequencies (dashed lines) from the double-sided representation are shown as upper sidebands with respect to the pump harmonics. The input signal power was chosen to be -130 dBm such that the higher order sidebands of the Floquet JTWPA are visible on the spectrum, and the amplification results in negligible pump depletion.

Thus, they would always predict an ideal quantum efficiency for a lossless JTWPA, inconsistent with experimental observations [3]. To accurately model the system dynamics and the quantum efficiency of JTWPAs, we go beyond the two-mode model and choose a larger number of modes m to account for the effects of the interacting sidebands modes [22], [33], [41], [42]. We find that an accurate computation of quantum efficiency for typical JTWPA designs requires $m \geq 6$. For arbitrary positive signal and pump frequencies ω_s and ω_P respectively, a discrete ordered set of frequencies – that can be positive or negative – defines the k-th signal/idler frequency according to

$$\omega_k \equiv 2k\omega_P + \omega_s, \qquad (1)$$

for $k \in \{-\lfloor m/2 \rfloor, \ldots, \lfloor (m-1)/2 \rfloor\}$, where $\lfloor . \rfloor$ is the floor function, and $\omega_0 = \omega_s$. The set $\{\omega_k\}$ defined by (1) follows from the cosine potential energy of unbiased Josephson junctions [43] and the linearization with respect to the signal and generated idlers. Equation (1) defines a double-sided intermodulation spectrum corresponding to first-order mixing of the signal with the odd harmonics of the pump frequency.

We work in conventional power-wave variables defined by the linear combinations of complex voltages and currents at each port according to $a_n = (V_n + Z_0 I_n)/(2\sqrt{Z_0})$ and $b_n = (V_n - Z_0 I_n)/(2\sqrt{Z_0})$, with Z_0 being a fixed characteristic reference impedance taken conventionally to be 50 Ω. The relationship among incident waves a_{q,ω_k} at port q at frequency ω_k and scattered waves b_{p,ω_j} at port p at frequency ω_j is given by

$$b_{p,\omega_j} = \sum_{\substack{q=1,2 \\ k=-\lfloor m/2 \rfloor, \ldots, \lfloor (m-1)/2 \rfloor}} X_{p,\omega_j;q,\omega_k} a_{q,\omega_k}, \qquad (2)$$

where $p \in \{1, 2\}$ represents the two ports and $j \in \{-\lfloor m/2 \rfloor, \lfloor (m-1)/2 \rfloor\}$ is the mode index. Moreover, the coefficients in (2) can be identified as the elements of the double-sided X-parameter sensitivity matrix of dimension $2m \times 2m$ [44] for incommensurate signal and pump frequencies, expressible as

$$X_{p,\omega_j;q,\omega_k} \equiv \lim_{a_{q,\omega_k} \to 0} \frac{b_{p,\omega_j}\left(|A^{\text{pump}}|\right)}{a_{q,\omega_k}}. \qquad (3)$$

The X-parameters in (2) and (3) are nonlinear functions of the magnitude of the pump amplitude. The X-parameters are computed, not from (3), but rather by the simulator as part of the harmonic balance solution of the system circuit equations in the frequency domain, utilizing the spectral Jacobian computed from the well-defined partial derivatives of the constitutive relations of the circuit elements (Josephson junctions and linear capacitors and inductors) of the JTWPA. The resulting X-parameters are the wave-variable representation of the classical conversion matrix formalism usually expressed in admittance or impedance representation [45].

The full nonlinear X-parameter formalism, including the measurement science and the nonlinear mathematical model implemented in the ADS simulator, are much more general than the limited discussion of the X-parameter sensitivity matrix analysis that is the main focus of this work. The X-parameter sensitivity matrix introduced in (2) and (3) is just the spectrally linearized portion of a more complete X-parameter model that includes the contributions to the scattered waves from each port due to the pump and its harmonics in addition to the terms linear in the signal phasor and created idlers. Together, these terms account for all the spectral components shown in Fig. 2. More generally and most importantly, X-parameter models build into the mathematical representation

the required phase relationships among commensurately related signals, such as the pump harmonics and any reflections thereof, as required by the underlying physical constraint of time-invariance of the component. For example, the phasor at port p at the n-th pump harmonic can be shown to have the general X-parameter form $X_{p,n\omega_p}^F (|A_p|) e^{ni\theta(A_p)}$. These are the Fourier coefficients of waves that have, by construction, the required phase dependence to ensure that when the input signal is delayed by any amount the same output response is obtained as previously, but now delayed by precisely the same interval as the input delay. The time-invariant constraint on the mathematical model is not satisfied for a general complex-valued nonlinear function of the complex input phasor A_p. X-parameter models identified from measurements require special nonlinear calibration and a cross-frequency phase calibration to identify the time-invariant intrinsic device characteristics. The co-variant mathematical formulation of the model terms guarantees that any simulations with the model will behave correctly for the entire equivalence class of signals delayed by an arbitrary time. In some cases, such as a JPA, where the signal may be incident at a harmonic of the pump, the explicit phase-dependence of the amplification is properly taken into account by the X-parameter model [46].

B. From Classical to Quantum Properties

The above analysis applies to the linearized dynamics of a nonlinear classical circuit driven by a strong, periodically time-varying pump. The linearized power-wave solutions can then be mapped into the quantum field ladder operator basis [22] to properly calculate the quantum statistics of linear amplifiers [47]. This is accomplished by defining quantum X-parameters according to (4). The transformation from the classical power wave basis to the quantum ladder operator basis [48] can be justified rigorously by deriving the input-output relations in the field ladder operator basis from the JTWPA system circuit Lagrangian and the corresponding Heisenberg equations of motions [22], [39]. Alternatively, this transformation can be understood classically as a consequence of the Manley-Rowe relations which are an expression of energy conservation [49].

$$x_{p,\omega_j;q,\omega_k} \equiv X_{p,\omega_j;q,\omega_k} \sqrt{\left|\frac{\omega_k}{\omega_j}\right|}. \tag{4}$$

Equation (5) describes the additional constraint on the quantum X-parameters to preserve the underlying quantum commutation relations of bosonic operators [22], [47], [50]–[52]. The quantum X-parameters numerically evaluated from the simulator have been checked to satisfy (5) within numerical precision, supporting the correctness of our framework.

$$\sum_{\substack{q=1,2 \\ k=-\lfloor m/2 \rfloor,...,\lfloor (m-1)/2 \rfloor}} \mathrm{sgn}\,(\omega_k) \left|x_{p,\omega_j;q,\omega_k}\right|^2 = \mathrm{sgn}\,(\omega_j). \tag{5}$$

C. Quantum Efficiency from Quantum X-parameters

Quantum efficiency (QE) is defined as the ratio of the output to input signal-to-noise ratio (SNR) [22], [23]. In the case

when each of the input modes has a minimum vacuum noise of half a quantum, QE for a pair of input and output modes, a_{q,ω_l} and b_{p,ω_n}, represents the ratio of the noise in the output mode b_{p,ω_n} originating from the input mode a_{q,ω_l} to the sum of noise from all input modes. A closed-form expression for the quantum efficiency in terms of the quantum X-parameters is given by

$$\mathrm{QE}_{p,\omega_n;q,\omega_l} = \frac{|x_{p,\omega_n;q,\omega_l}|^2}{\sum\limits_{\substack{q'=1,2 \\ k=-\lfloor m/2 \rfloor,...,\lfloor (m-1)/2 \rfloor}} |x_{p,\omega_n;q',\omega_k}|^2}, \tag{6}$$

which is a matrix, analogous to the noise figure matrix defined in [41]. Quantities of particular interest for transmission-mode quantum-limited amplifiers are $\mathrm{QE}_{2,\omega_0,1,\omega_0}$ and $\mathrm{QE}_{2,\omega_{-1},1,\omega_0}$ that define the quantum efficiency of the signal and the primary idler, respectively, for inputs at port 1 and outputs at port 2, including interactions with all m modes. Other entries in the QE matrix, such as $\mathrm{QE}_{2,\omega_1,1,\omega_0}$ and $\mathrm{QE}_{2,\omega_{-2},1,\omega_{-1}}$ define the quantum efficiency of devices functioning as frequency converters. For the uniform JTWPA design considered here, the number of modes needs to be at least six before the results converge to a level of 10^{-3}, confirming the limitation of two-mode models.

D. Quantum Efficiency with Dissipation

The impedance of a capacitor of capacitance C_d with dielectric loss tangent $\tan \delta$ can be modeled as an effective series resistance plus a standard capacitor

$$Z_d(\omega) = \frac{\tan \delta}{\omega C_d} + \frac{1}{j\omega C_d} \tag{7}$$

or $Y_d(\omega) = j\omega C_d / (1 + j \tan \delta)$ when expressed as an admittance, which is more efficient for simulation. The loss in the capacitor produces noise, which can be expressed as a noise current spectral density $\langle i_n^2 \rangle (\omega)$ generated in parallel with the admittance Y

$$\langle i_n^2 \rangle (\omega) = 4 \frac{\hbar\omega \coth (\hbar\omega/2kT)}{2} \mathrm{Re}\,[Y(\omega)]. \tag{8}$$

At non-cryogenic temeperatures and typical microwave frequencies it simplifies to the classical $4kT \mathrm{Re}\,[Y(\omega)]$; at $T = 0$, this simplifies to $4(\hbar\omega/2) \mathrm{Re}\,[Y(\omega)]$.

The noise power delivered to port p at frequency ω_n, due to the noise generated by all of the components in the system, is calculated using

$$P_{p,\omega_n}^{N,dut} = \sum_k \sum_d Z_{d,k;p,n} \langle i_{n:d,k}^2 \rangle Z_{d,k;p,n}^\dagger / \mathrm{Re}\,(Z_{p,n}) \tag{9}$$

where

- $k = -\lfloor m/2 \rfloor, \ldots, \lfloor (m-1)/2 \rfloor$;
- d is the set of all noise generating devices;
- $Z_{d,m;p,n} = \partial v_{p,n}/\partial i_{d,m}$ denotes the transimpedance from device d's current at frequency index m to the port p at frequency index n;

- $\left\langle i_{n:d,k}^2 \right\rangle$ is the noise correlation matrix due to device d at frequency index k;
- $Z_{p,n}$ is the impedance of port p at frequency index n.

The available noise power from input port q and frequency ω_l is given by

$$P_{q,\omega_l}^{N,in} = \hbar\omega_l \coth\left(\hbar\omega_l/2kT\right)/2. \tag{10}$$

The ratio of these two noise values, after frequency scaling to photon number units, represents the fraction of added noise power to input noise power

$$N_{p,\omega_n} = \frac{P_{p,\omega_n}^{N,dut}/|\hbar\omega_n|}{P_{q,\omega_l}^{N,in}/|\hbar\omega_l|}. \tag{11}$$

With a typical electrical length of tens of wavelengths, realistic JTWPA devices often have non-negligible propagation loss due to two-level-system defects in the dielectrics of the capacitors. Therefore, the quantum efficiency calculation at the presence of loss has to properly account for the excess noise introduced to the device output associated with dissipation, as dictated by the fluctuation-dissipation theorem [53]. The quantum efficiency of a JTWPA with dissipation can be expressed by adding the noise ratio N_{p,ω_n} to the denominator of (6)

$$\mathrm{QE}_{p,\omega_n;q,\omega_l} = \frac{|x_{p,\omega_n;q,\omega_l}|^2}{\displaystyle\sum_{\substack{q'=1,2 \\ k=-\lfloor m/2 \rfloor,\ldots,\lfloor (m-1)/2 \rfloor}} |x_{p,\omega_n;q',\omega_k}|^2 + N_{p,\omega_n}}. \tag{12}$$

The noise power response at the input and output ports can be calculated from the Green's function scattering matrices [22] or using adjoint methods in classical circuit analysis [54], [55]. Signal dissipation at each node can be understood as coherent scattering into a semi-infinite transmission line channel, and the associated noise is at the same time introduced into the system by a noise source radiating from the opposite side of the transmission line channel. Alternatively, the noise power response ratio can be conceptually understood as additional magnitude square quantum X-parameter terms if each internal node is also assigned a port in an extended X-parameter analysis.

Analogous to (5), (13) specifies the constraint on the noise power response terms and X-parameters to conserve bosonic commutation relations in the presence of loss.

$$\sum_{\substack{k=-\lfloor m/2 \rfloor, \\ \ldots,\lfloor (m-1)/2 \rfloor}} \mathrm{sgn}\left(\omega_k\right) \left(\sum_{q=1,2} \left|x_{p,\omega_j;q,\omega_k}\right|^2 + N_{p,\omega_n} \right) = \mathrm{sgn}\left(\omega_j\right) \tag{13}$$

III. Results

A. Gain vs Signal Frequency and Pump Power

Each X-parameter matrix element is the power or conversion gain for one of the small incident signals. Specifically, the diagonal elements are power gains and the off-diagonals are conversion gains. For example, $|X_{2,\omega_0;1,\omega_0}|^2$ gives the power gain of the signal at the output port relative to the input port, and $\left|X_{2,\omega_{-1};1,\omega_0}\right|^2$ gives the conversion gain of the primary ($k = -1$) idler at the output port with respect to the signal incident at the input port.

Fig. 3 shows the gain of the signal and primary idler for the two JTWPA designs [3], [22] evaluated in this work. In both cases, the results obtained using frequency domain X-parameter analysis are consistent with nonlinear time-domain analysis using WRSPICE [56] once the maximum phase change per step is reduced to 0.01 from the default of $\pi/5$ through the WRSPICE configuration parameter dphimax. On a desktop computer (AMD Ryzen 9 3950X 16-Core Processor), simulating gain and quantum efficiency for all 131 signal frequencies using JosephsonCircuits.jl with $m = 10$ takes 3.9 and 2.5 seconds for the uniform and Floquet designs, respectively. In the Julia model, simulation time approximately doubles when dissipation is included. In WRSPICE, simulating the gain for a single frequency takes 13.3 and 8.2 seconds for the uniform and Floquet designs, respectively, and three simulations are required to extract the complex scattering parameters (pump only and pump + signal with two different phases). Simulating the required terms in the X parameter matrix to compute the quantum efficiency matrix ($2 \cdot 2 \cdot m \cdot 131 + 1$ simulations) for 131 signal frequencies in WRSPICE would take an estimated 19.5 and 12.0 hours, respectively, which is order of 10,000 times slower than the Julia harmonic balance code. WRSPICE also is unable to model lossy capacitors. The ADS and MIT frequency domain analyses show excellent agreement. The MIT code, written specifically for these types of circuits, is naturally faster than a general-purpose microwave circuit simulator like ADS.

For periodic or quasi-periodic parametric circuits, harmonic balance (HB) is more accurate and faster than time-domain solutions that integrate the ordinary differential equations until steady-state before performing Fourier analysis, with the linearization being approximated by subtracting the large-signal pump solution from a time-domain solution that includes small-signal tones as well.

B. Quantum Efficiency and the Number of Interacting Modes

The signal quantum efficiency of the two considered JTWPA designs simulated with different number of modes m at $\omega_0/(2\pi) = 6\,\mathrm{GHz}$ is presented in Table II. The QE values here are normalized by the corresponding ideal quantum efficiency at the same power gain G to compare amplifier performance at similar but nonidentical gains [22], [23]:

$$\mathrm{QE}_{\mathrm{ideal}}(G) = \begin{cases} \frac{1}{2-1/G}, & |G| \geq 1, \\ 1, & |G| < 1. \end{cases} \tag{14}$$

Consequently, ideal quantum-limited amplifiers have a normalized quantum efficiency of 100% using this definition. For the uniform JTWPA design, the quantum efficiency normalized to the ideal converges to approximately 80.4% at $m = 6$,
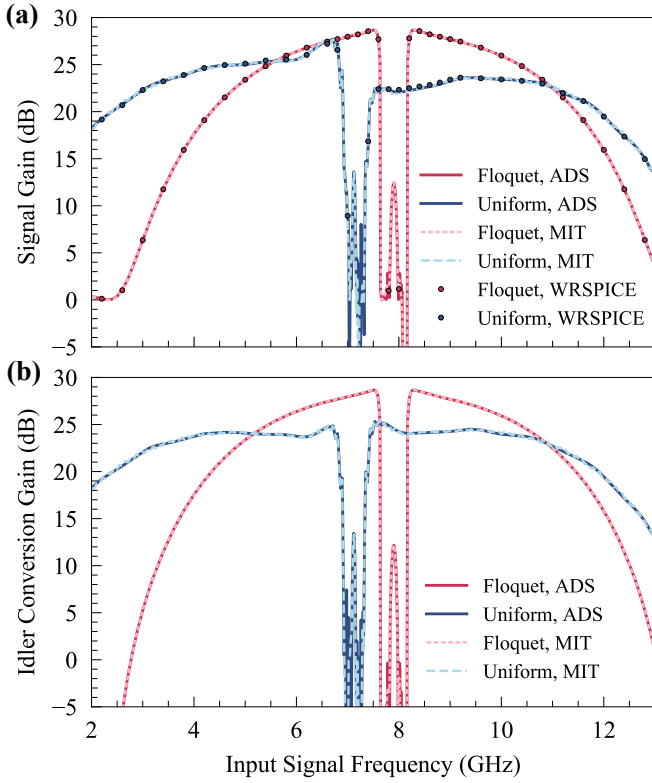
Fig. 3. Simulated signal (a) and idler (b) gain versus signal frequency for two JTWPA designs, the uniform design (blue) and the Floquet design (red).
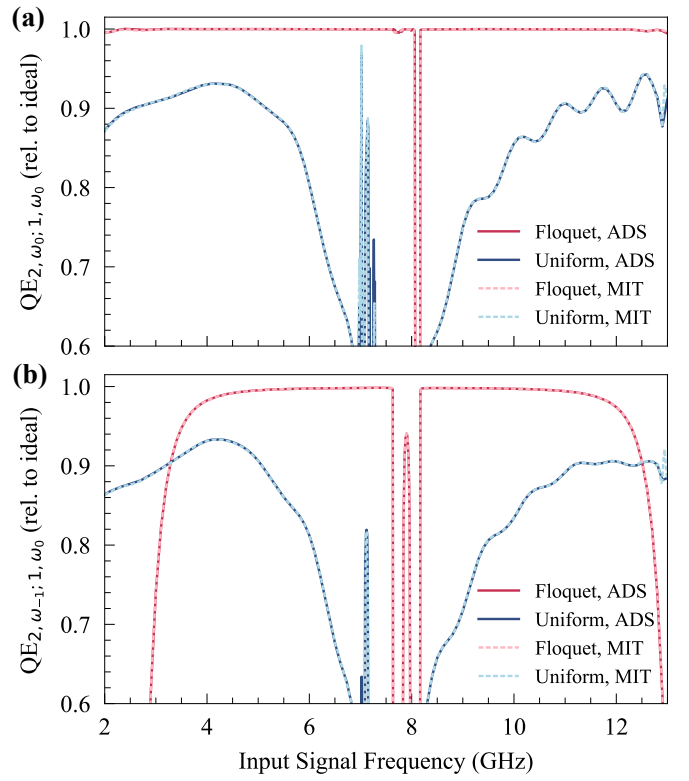

Fig. 4. The simulated (a) signal and (b) idler quantum efficiencies, $QE_{2,\omega_0,1,\omega_0}$ and $QE_{2,\omega_{-1},1,\omega_0}$, respectively, of the uniform (blue) and Floquet JTWPA (red) designs normalized by those of an ideal quantum-limited amplifier at the same power gain G specified by (14).

whereas the Floquet-mode JTWPA design converges to approximately 100.0% at $m = 4$. To the authors' knowledge, this is the first quantum efficiency calculation of a circuit quantum electrodynamics device performed in a commercial circuit simulator.

Fig. 4 shows the signal and idler quantum efficiency $QE_{2,\omega_0,1,\omega_0}$ and $QE_{2,\omega_{-1},1,\omega_0}$ from (6), normalized by the corresponding ideal quantum efficiency, as a function of the input signal frequency at $m = 10$. Our framework predicts normalized signal quantum efficiency of 81.35% at $\omega_0/(2\pi) = 5.984$ GHz for the uniform JTWPA design, consistent with the experimentally inferred value, factoring out dissipation, of 85% in [3]. Our framework likewise yields a near-ideal quantum efficiency ($\sim 99.9\%$) performance over the entire working bandwidth of the Floquet JTWPA design, corroborating the predictions of the wave-equation-based model in [22] by also accounting for both the large number of interacting sideband modes and the discreteness of device design. The ability to accurately predict and differentiate the quantum noise

performance of near-quantum-limited and quantum-limited amplifiers makes our framework an invaluable tool for the design and optimization of quantum parametric devices.

C. Quantum Efficiency Calculation in the Presence of Loss

Fig. 5 shows the signal gain and quantum efficiency of the Floquet JTWPA design at several dielectric loss tangent values ranging from 10^{-6} to $3 \cdot 10^{-3}$, pertinent to coplanar-waveguide capacitors and silicon dioxide or alumina parallel-plate capacitors [3], [20], respectively. We scale the input pump current in each trace by a factor of $(1 + 125 \tan\delta)$ to maintain a similar level of gain across different $\tan\delta$ value simulations for comparison. The quantum efficiency values predicted by ADS and the Julia model again show excellent agreement with each other, and the quantum efficiency decreases with increased dielectric loss tangent as expected. Different from the prediction in [22] where the same input pump current and pump profile were assumed across different loss levels and resulted in significantly reduced signal gain, the Floquet TWPA has a predicted quantum efficiency close to 90% even at a loss level $\tan\delta = 3 \times 10^{-3}$ of silicon dioxide parallel-plate capacitors [3], [34]. Furthermore, the quantum efficiency of the Floquet TWPA design at a certain loss level can be improved further by optimizing its nonlinearity profile to balance the incoherent material loss and coherent sideband loss contributions, making the demonstration of a near-term

TABLE II
SIMULATED QUANTUM EFFICIENCY VS NUMBER OF MODES m

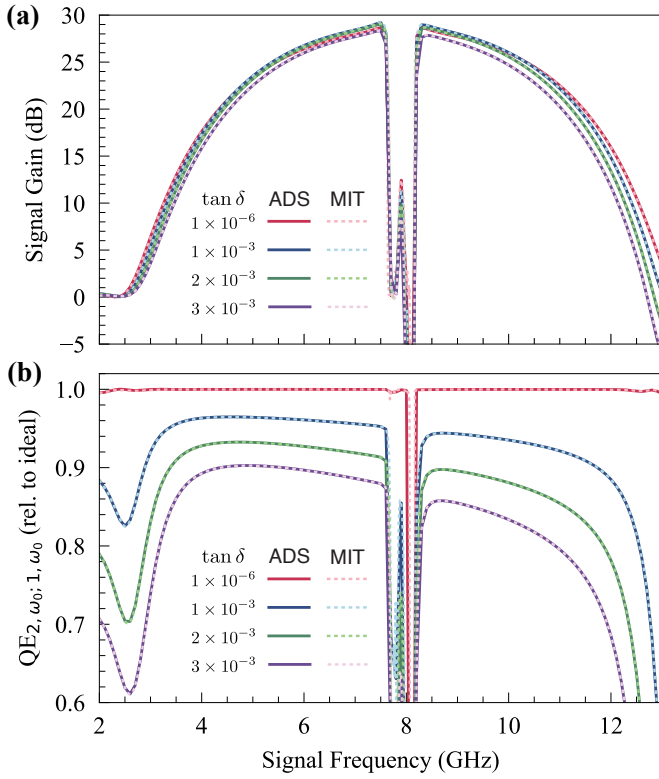| Design	$m=2$	$m=4$	$m=6$	$m=8$	$m=10$
Uniform	0.999554	0.772218	0.804080	0.804028	0.804109
Floquet	0.999998	0.999863	0.999857	0.999856	0.999856

Fig. 5. The simulated (a) gain and (b) quantum efficiency spectra of the Floquet JTWPA design at several dielectric loss tangent values relevant to existing fabrication processes. The quantum efficiency is normalized by those of an ideal quantum-limited amplifier having the same gain ($1/(2 - 1/G)$) [22] as in Fig. 4.

advantage of Floquet TWPA possible with current fabrication processes.

In addition, the bosonic commutation relations of the output modes at the presence of loss specified in (13) were numerically verified to be ± 1 within numerical precision as required by quantum mechanics, suggesting the validity of both approaches as quantum-mechanically consistent models.
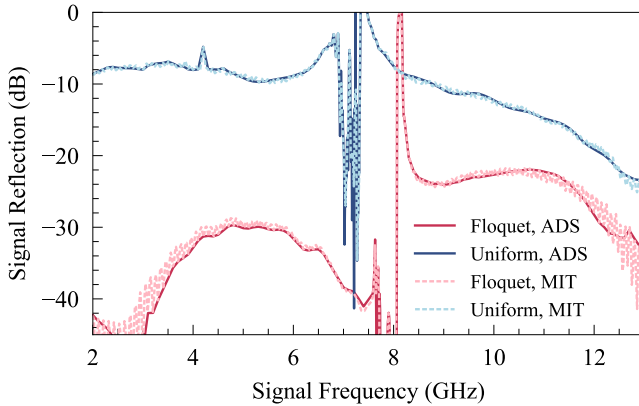

Fig. 6. The signal S_{11} (input match to $50\,\Omega$ environment) of the uniform and Floquet JTWPA designs.
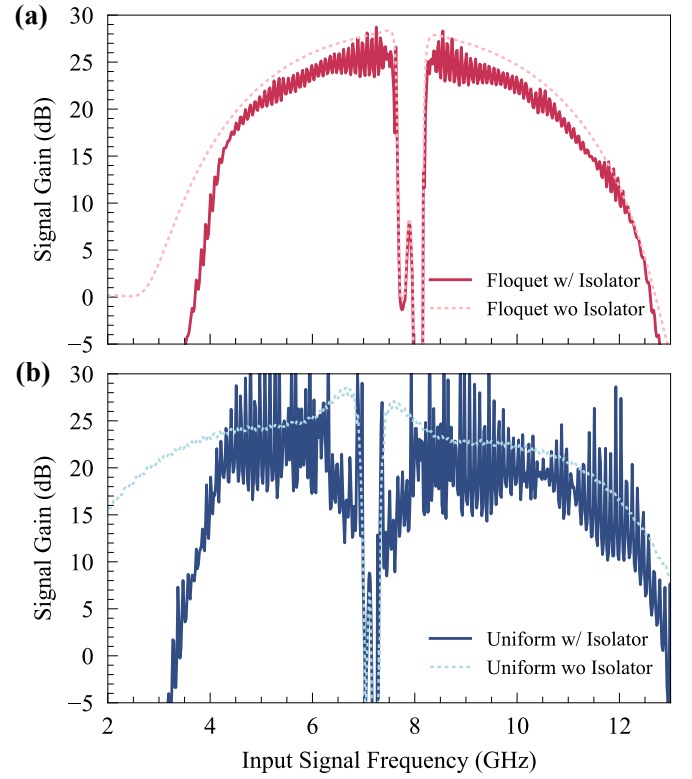

Fig. 7. Simulated gain spectra of the (a) Floquet and (b) uniform JTWPA designs when placed in between a pair of 4-12 GHz commercial double-junction circulators, a common configuration in superconducting qubit measurement setup. A dielectric loss tangent of $\tan\delta = 3 \cdot 10^{-3}$ is used for both TWPA designs, and the input pump current for the Floquet and uniform TWPA are scaled by $(1 + 125\tan\delta)$ and $(1 + 170\tan\delta)$, respectively, to maintain $> 20\,\mathrm{dB}$ gain levels similar to those in Fig. 3.

D. Mismatch Effects

We can simulate the interaction of the JTWPA with neighboring components (e.g. cables to HEMT amplifiers at higher temperature stages of the measurement setup), out-of-band impedance effects, and the degree to which the input of the JTWPA is matched to the signal over the operating frequency range. An example is shown in Fig. 6, where we plot the signal input mismatch of the chosen JTWPA designs to a $50\,\Omega$ environment as a function of signal frequency. We observe that despite having similar impedance and signal gain level, the uniform conventional JTWPA design results in significantly larger reflections compared to the Floquet JTWPA designs, further confirming the predictions in [22] using a circuit model. The capability to quantitatively evaluate and engineer input and output matches provides valuable guidance in realizing applications such as on-chip integration of quantum-limited amplifiers.

Impedance mismatch effects can be also straightforwardly accounted for and modeled in our framework. Significant out-of-band impedance mismatch occurs in a qubit readout chain as dictated by the Bode-Fano limit [57], [58], when in-band mismatch is optimized to maximize measurement efficiency and minimize qubit dephasing caused by undesirable back

reflections. Nonlinear devices may be adversely affected by out-of-band impedance mismatch on sideband modes [22]. In Fig. 7 we plot the predicted gain performance of the two JTWPA designs using a realistic dielectric loss tangent of $\tan\delta = 3\cdot10^{-3}$ and under the realistic impedance environment resulted from a Quinstar commercial 4-12 GHz circulator (model QCY-G0401202AM) commonly used in superconducting qubit measurements using ADS. In ADS, the measured scattering parameters of the circulator considered are imported and used to directly specify the response of the created components. The JTWPA and circulators are simulated together to predict the performance in a realistic superconducting qubit measurement setup. Consistent with the predictions in [22] using a simplified constant out-of-band impedance model, the uniform and Floquet TWPA designs show drastically different behaviors at the presence of out-of-band impedance caused by circulators. The uniform JTWPA shows instability and significantly increased gain ripples from parametric oscillations, qualitatively agreeing with the experimental observations that are not captured by models assuming a constant 50 Ω port impedance.

The gain profile of the Floquet JTWPA is less affected by the presence of the isolators than the gain profile of the uniform JTWPA. The small ripples are caused by both the large round trip gain (~ 25 dB) and the in-band impedance mismatch of the isolators. The slightly reduced bandwidth is caused by the 4-12 GHz working bandwidth of the isolators. Compared to the uniform TWPA designs, Floquet TWPA designs are much less sensitive to non-ideal out-of-band impedance mismatch due to more than an order of magnitude suppression of higher pump harmonics and sideband generation as seen in Fig. 2. The ability of our analysis framework to model different in- and out-of-band impedance environments will be valuable for both modeling and designing the parametric devices under realistic experimental setups.

E. Nonlinear Signal Effects

The above treatment and results are based on an exact numerical linearization around the periodically time-varying solution of the JTWPA when excited by the large pump tone. We note that exact linearization is required for the standard quantum statistics analysis of linear amplifiers to hold [47], [51]. When the signal power to be amplified becomes large enough there will arise compression and higher signal order intermodulation effects that need to be considered. Nonlinear signal effects are particularly detrimental in the context of frequency-multiplexed qubit readout, as they set an upper bound on the maximum number of qubits that can be read out simultaneously. These can be accounted for classically by replacing the linearized harmonic balance calculations with full two-tone harmonic balance analyses in which higher than first order in the signal and idler intermodulation products are simulated. A quantum mechanical analysis of these nonlinear signal effects is beyond the scope of this work.

Fig. 8 shows the compression characteristics of the signal gain versus input signal power for the uniform and Floquet
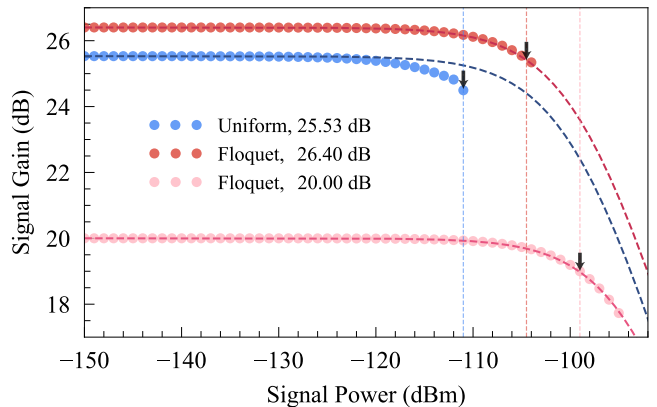

Fig. 8. Gain compression and P_{1dB} of the two analyzed JTWPA designs. The dots are simulated using a full two-tone harmonic balance model in ADS, whereas the dashed lines are calculated using the analytical pump depletion formula in [59] (see main text). The P_{1dB} points are marked using arrows.

JTWPA designs. Two signal gain compression curves are presented for the Floquet JTWPA at two different pump powers to highlight the dependence of the 1-dB gain compression point on the magnitude of the small signal gain. The gain compression points, P_{1dB}, are -104.5 dBm and -99 dBm at 26.40 dB and 20.00 dB gain, respectively. The simulated P_{1dB} of the uniform JTWPA design at 25.53 dB gain is -111 dBm. We note that this value is smaller than the reported value in [3] of -99 dBm due to differences in the operating pump configuration and small signal gain, the non-negligible material loss, and the non-ideal out-of-band impedance mismatch [22] in the measured device.

We observe that the simulated signal gain compression values of the Floquet JTWPA design using the full two-tone harmonic balance simulations show excellent agreement with those predicted by the approximate analytical formula $G(P_s) = G_0/(1 + 2G_0 P_s/P_p)$ [59], which captures the effect of pump depletion from the signal and the principal idler. This suggests that, just as the case for ideal two-mode parametric amplifiers, pump depletion is the dominant source for gain compression for the Floquet JTWPA designs, despite their more complicated circuit profiles. In contrast, the gain compression profile of the considered uniform JTWPA design deviates from that of the analytical pump depletion formula and leads to a lower P_{1dB} value. This may result from the additional pump power consumption due to the generation of higher pump harmonics and higher-order sideband modes by the uniform TWPA design, both of which are more than an order of magnitude larger than in the Floquet TWPA as shown in Fig. 2.

IV. CONCLUSION

A unified design and simulation methodology for generic multi-port, multi-frequency parametric circuits in the presence of loss based on quantum-adapted X-parameter analysis has been presented with example simulations for JTWPAs, a key amplifier technology widely used for superconducting qubit

readout and quantum sensing. Each X-parameter provides a mapping between the input at a frequency and port to the output at a specific frequency and port, among the set of modes considered in the analysis. Explicit formulas for the quantum efficiency with and without dissipation are presented in terms of quantum X-parameters and evaluated for two distinct JTWPA designs for the first time using a commercial circuit simulator. The gain and quantum efficiency results are consistent among ADS, JosephsonCircuits.jl, and WRSPICE. The presented analysis flow is applicable to all commercial harmonic balance solvers and is already implemented in a recent commercial release of ADS that includes a Josephson junction model. Compared to Fourier analysis of a time domain simulation, these methods more rapidly and accurately simulate the multiple interacting signal and idler modes that are required to predict JTWPA quantum efficiency. This analysis more realistically captures the discrete nature of the JTWPA layout (discrete components that can vary along the structure) than analytic continuum or coupled mode theory models.

Detailed layout-dependent parasitic effects, such as bends, can be modeled in the same design environment using EM analysis. The full power of commercial nonlinear circuit simulators is now available to optimize JTWPAs and other devices based on parametric processes (e.g. circulators and kinetic inductance amplifiers) for key quantum applications.

V. Future work

Extending the interoperable simulation, modeling, and measurement X-parameter use model [60] to include JTWPAs and similar quantum devices with their full characteristics including dissipation and fabrication variation is the ultimate objective. Future work therefore includes calibrated nonlinear X-parameter measurements of real JTWPAs in a cryogenic environment. This will provide a direct comparison of simulations and calibrated nonlinear measured JTWPA performance characteristics, such as gain, quantum efficiency, and out-of-band impedance effects. An enhancement to the existing X-parameter model within Keysight PathWave Advanced Design System (ADS) will enable consumption of simulated and/or measured X-parameters of the JTWPA to be directly consumed as a behavioral model block for the design of qubit readout chains. JTWPA component manufacturers could then provide X-parameter models to quantum chip designers without compromising design IP, and consumers of JTWPA components can specify requirements based on X-parameters and QE derived from them. Users of JTWPAs and other parametric devices can compare prospective technologies in the simulator using the X-parameter behavioral model in a realistic environment including the full readout chain.

Acknowledgment

References

[1] D. M. Pozar, *Microwave engineering*. John wiley & sons, 2011.

[2] B. Yurke, L. R. Corruccini, P. G. Kaminsky, L. W. Rupp, A. D. Smith, A. H. Silver, R. W. Simon, and E. A. Whittaker, "Observation of parametric amplification and deamplification in a Josephson parametric amplifier," *Phys. Rev. A*, vol. 39, no. 5, pp. 2519–2533, Mar 1989.

[3] C. Macklin, K. O'Brien, D. Hover, M. E. Schwartz, V. Bolkhovsky, X. Zhang, W. D. Oliver, and I. Siddiqi, "A near–quantum-limited Josephson traveling-wave parametric amplifier," *Science*, vol. 350, no. 6258, pp. 307–310, Oct 2015.

[4] M. Mirhosseini, A. Sipahigil, M. Kalaee, and O. Painter, "Superconducting qubit to optical photon transduction," *Nature*, vol. 588, no. 7839, pp. 599–603, Dec. 2020.

[5] D. P. DiVincenzo, "The physical implementation of quantum computation," *Fortschritte der Physik*, vol. 48, no. 9-11, pp. 771–783, 2000.

[6] A. Wallraff, D. I. Schuster, A. Blais, L. Frunzio, R.-S. Huang, J. Majer, S. Kumar, S. M. Girvin, and R. J. Schoelkopf, "Strong coupling of a single photon to a superconducting qubit using circuit quantum electrodynamics," *Nature*, vol. 431, pp. 162–167, 2004. [Online]. Available: https://doi.org/10.1038/nature02851

[7] M. Kjaergaard, M. E. Schwartz, J. Braumüller, P. Krantz, J. I.-J. Wang, S. Gustavsson, and W. D. Oliver, "Superconducting qubits: Current state of play," *Annual Review of Condensed Matter Physics*, vol. 11, no. 1, pp. 369–395, 2020. [Online]. Available: https://doi.org/10.1146/annurev-conmatphys-031119-050605

[8] J. M. Hornibrook, J. I. Colless, A. C. Mahoney, X. G. Croot, S. Blanvillain, H. Lu, A. C. Gossard, and D. J. Reilly, "Frequency multiplexing for readout of spin qubits," *Applied Physics Letters*, vol. 104, no. 10, p. 103108, 2014. [Online]. Available: https://doi.org/10.1063/1.4868107

[9] X. Mi, M. Benito, S. Putz, D. M. Zajac, J. M. Taylor, G. Burkard, and J. R. Petta, "A coherent spin–photon interface in silicon," *Nature*, vol. 555, pp. 599–603, 2018. [Online]. Available: https://doi.org/10.1038/nature25769

[10] A. J. Landig, J. V. Koski, P. Scarlino, U. C. Mendes, A. Blais, C. Reichl, W. Wegscheider, A. Wallraff, K. Ensslin, and T. Ihn, "Coherent spin–photon coupling using a resonant exchange qubit," *Nature*, vol. 560, pp. 179–184, 2018. [Online]. Available: https://doi.org/10.1038/s41586-018-0365-y

[11] P. Krantz, M. Kjaergaard, F. Yan, T. P. Orlando, S. Gustavsson, and W. D. Oliver, "A quantum engineer's guide to superconducting qubits," *Applied Physics Reviews*, vol. 6, no. 2, p. 021318, 2019. [Online]. Available: https://doi.org/10.1063/1.5089550

[12] M. A. Castellanos-Beltran and K. W. Lehnert, "Widely tunable parametric amplifier based on a superconducting quantum interference device array resonator," *Appl. Phys. Lett.*, vol. 91, no. 8, p. 083509, Aug 2007.

[13] T. Yamamoto, K. Inomata, M. Watanabe, K. Matsuba, T. Miyazaki, W. D. Oliver, Y. Nakamura, and J. S. Tsai, "Flux-driven Josephson parametric amplifier," *Appl. Phys. Lett.*, vol. 93, no. 4, p. 042510, Jul 2008.

[14] N. Bergeal, F. Schackert, M. Metcalfe, R. Vijay, V. E. Manucharyan, L. Frunzio, D. E. Prober, R. J. Schoelkopf, S. M. Girvin, and M. H. Devoret, "Phase-preserving amplification near the quantum limit with a Josephson ring modulator," *Nature*, vol. 465, pp. 64–68, May 2010.

[15] B. H. Eom, P. K. Day, H. G. LeDuc, and J. Zmuidzinas, "A wideband, low-noise superconducting amplifier with high dynamic range," *Nat. Phys.*, vol. 8, pp. 623–627, Aug 2012.

[16] M. R. Vissers, R. P. Erickson, H.-S. Ku, L. Vale, X. Wu, G. C. Hilton, and D. P. Pappas, "Low-noise kinetic inductance traveling-wave amplifier using three-wave mixing," *Appl. Phys. Lett.*, vol. 108, no. 1, p. 012601, Jan 2016.

[17] M. Malnou, M. R. Vissers, J. D. Wheeler, J. Aumentado, J. Hubmayr, J. N. Ullom, and J. Gao, "Three-Wave Mixing Kinetic Inductance Traveling-Wave Amplifier with Near-Quantum-Limited Noise Performance," *PRX Quantum*, vol. 2, no. 1, p. 010302, Jan 2021.

[18] K. O'Brien, C. Macklin, I. Siddiqi, and X. Zhang, "Resonant phase matching of josephson junction traveling wave parametric amplifiers," *Phys. Rev. Lett.*, vol. 113, p. 157001, Oct 2014. [Online]. Available: https://link.aps.org/doi/10.1103/PhysRevLett.113.157001

[19] T. C. White, J. Y. Mutus, I.-C. Hoi, R. Barends, B. Campbell, Y. Chen, Z. Chen, B. Chiaro, A. Dunsworth, E. Jeffrey, J. Kelly, A. Megrant, C. Neill, P. J. J. O'Malley, P. Roushan, D. Sank, A. Vainsencher, J. Wenner, S. Chaudhuri, J. Gao, and J. M. Martinis, "Traveling wave

parametric amplifier with Josephson junctions using minimal resonator phase matching," *Appl. Phys. Lett.*, vol. 106, no. 24, p. 242601, Jun 2015.

[20] L. Planat, A. Ranadive, R. Dassonneville, J. Puertas Martínez, S. Léger, C. Naud, O. Buisson, W. Hasch-Guichard, D. M. Basko, and N. Roch, "Photonic-crystal josephson traveling-wave parametric amplifier," *Phys. Rev. X*, vol. 10, p. 021021, Apr 2020. [Online]. Available: https://link.aps.org/doi/10.1103/PhysRevX.10.021021

[21] A. Ranadive, M. Esposito, L. Planat, E. Bonet, C. Naud, O. Buisson, W. Guichard, and N. Roch, "Kerr reversal in Josephson meta-material and traveling wave parametric amplification," *Nat. Commun.*, vol. 13, no. 1737, pp. 1–9, Apr. 2022.

[22] K. Peng, M. Naghiloo, J. Wang, G. D. Cunningham, Y. Ye, and K. P. O'Brien, "Floquet-mode traveling-wave parametric amplifiers," *PRX Quantum*, vol. 3, p. 020306, Apr 2022. [Online]. Available: https://link.aps.org/doi/10.1103/PRXQuantum.3.020306

[23] S. Boutin, D. M. Toyli, A. V. Venkatramani, A. W. Eddins, I. Siddiqi, and A. Blais, "Effect of higher-order nonlinearities on amplification and squeezing in josephson parametric amplifiers," *Phys. Rev. Applied*, vol. 8, p. 054030, Nov 2017. [Online]. Available: https://link.aps.org/doi/10.1103/PhysRevApplied.8.054030

[24] C. Eichler and A. Wallraff, "Controlling the dynamic range of a Josephson parametric amplifier," *EPJ Quantum Technol.*, vol. 1, no. 1, pp. 1–19, Dec 2014.

[25] J. Y. Mutus, T. C. White, R. Barends, Y. Chen, Z. Chen, B. Chiaro, A. Dunsworth, E. Jeffrey, J. Kelly, A. Megrant, C. Neill, P. J. J. O'Malley, P. Roushan, D. Sank, A. Vainsencher, J. Wenner, K. M. Sundqvist, A. N. Cleland, and J. M. Martinis, "Strong environmental coupling in a Josephson parametric amplifier," *Appl. Phys. Lett.*, vol. 104, no. 26, p. 263513, Jul 2014.

[26] T. Roy *et al.*, "Broadband parametric amplification with impedance engineering: Beyond the gain-bandwidth product," *Appl. Phys. Lett.*, vol. 107, no. 26, p. 262601, Dec 2015.

[27] N. E. Frattini, V. V. Sivak, A. Lingenfelter, S. Shankar, and M. H. Devoret, "Optimizing the Nonlinearity and Dissipation of a SNAIL Parametric Amplifier for Dynamic Range," *Phys. Rev. Appl.*, vol. 10, no. 5, p. 054020, Nov 2018.

[28] O. Naaman, D. G. Ferguson, A. Marakov, M. Khalil, W. F. Koehl, and R. J. Epstein, "High saturation power josephson parametric amplifier with ghz bandwidth," in *2019 IEEE MTT-S International Microwave Symposium (IMS)*, 2019, pp. 259–262.

[29] V. V. Sivak, S. Shankar, G. Liu, J. Aumentado, and M. H. Devoret, "Josephson Array-Mode Parametric Amplifier," *Phys. Rev. Appl.*, vol. 13, no. 2, p. 024014, Feb 2020.

[30] O. Yaakobi, L. Friedland, C. Macklin, and I. Siddiqi, "Parametric amplification in josephson junction embedded transmission lines," *Phys. Rev. B*, vol. 87, p. 144301, Apr 2013. [Online]. Available: https://link.aps.org/doi/10.1103/PhysRevB.87.144301

[31] A. L. Grimsmo and A. Blais, "Squeezing and quantum state engineering with Josephson travelling wave amplifiers," *npj Quantum Inf.*, vol. 3, no. 20, pp. 1–11, Jun 2017.

[32] M. Houde, L. C. G. Govia, and A. A. Clerk, "Loss asymmetries in quantum traveling-wave parametric amplifiers," *Phys. Rev. Applied*, vol. 12, p. 034054, Sep 2019. [Online]. Available: https://link.aps.org/doi/10.1103/PhysRevApplied.12.034054

[33] T. Dixon, J. W. Dunstan, G. B. Long, J. M. Williams, P. J. Meeson, and C. D. Shelly, "Capturing Complex Behavior in Josephson Traveling-Wave Parametric Amplifiers," *Phys. Rev. Appl.*, vol. 14, no. 3, p. 034058, Sep 2020.

[34] S. K. Tolpygo, V. Bolkhovsky, T. J. Weir, L. M. Johnson, M. A. Gouker, and W. D. Oliver, "Fabrication Process and Properties of Fully-Planarized Deep-Submicron Nb/Al– AlO$_x$/Nb Josephson Junctions for VLSI Circuits," *IEEE Transactions on Applied Superconductivity*, vol. 25, no. 3, pp. 1–12, 2015.

[35] J. M. Kreikebaum, K. P. O'Brien, A. Morvan, and I. Siddiqi, "Improving wafer-scale josephson junction resistance variation in superconducting quantum coherent circuits," *Superconductor Science and Technology*, vol. 33, no. 6, p. 06LT02, apr 2020. [Online]. Available: https://doi.org/10.1088/1361-6668/ab8617

[36] A. Osman, J. Simon, A. Bengtsson, S. Kosen, P. Krantz, D. P. Lozano, M. Scigliuzzo, P. Delsing, J. Bylander, and A. Fadavi Roudsari, "Simplified josephson-junction fabrication process for reproducibly high-performance superconducting qubits," *Applied Physics Letters*, vol. 118, no. 6, p. 064002, 2021. [Online]. Available: https://doi.org/10.1063/5.0037093

[37] D. Wan, S. Couet, X. Piao, L. Souriau, Y. Canvel, D. Tsvetanova, D. Vangoidsenhoven, A. Thiam, A. Pacco, A. Potočnik, M. Mongillo, T. Ivanov, J. Jussot, J. Verjauw, R. Acharya, F. Lazzarino, B. Govoreanu, and I. P. Radu, "Fabrication and room temperature characterization of trilayer junctions for the development of superconducting qubits on 300 mm wafers," *Japanese Journal of Applied Physics*, vol. 60, no. SB, p. SBBI04, mar 2021. [Online]. Available: https://doi.org/10.35848/1347-4065/abe5bb

[38] T. Sweetnam, D. Banys, V. Gilles, M. A. McCulloch, and L. Piccirillo, "Simulating the behaviour of travelling wave superconducting parametric amplifiers using a commercial circuit simulator," *arXiv*, Mar 2022. [Online]. Available: https://arxiv.org/abs/2203.09660

[39] K. P. O'Brien and K. Peng. (2022) JosephsonCircuits.jl. [Online]. Available: https://github.com/kpobrien/JosephsonCircuits.jl

[40] J. Y. Qiu, A. Grimsmo, K. Peng, B. Kannan, B. Lienhard, Y. Sung, P. Krantz, V. Bolkhovsky, G. Calusine, D. Kim, and other, "Sroadband Squeezed Microwaves and Amplification with a Josephson Traveling-Wave Parametric Amplifier," *arXiv*, Mar 2022. [Online]. Available: https://arxiv.org/abs/2201.11261

[41] C. J. McKinstrie, M. Yu, M. G. Raymer, and S. Radic, "Quantum noise properties of parametric processes," *Opt. Express*, vol. 13, no. 13, pp. 4986–5012, Jun 2005. [Online]. Available: http://www.opticsexpress.org/abstract.cfm?URI=oe-13-13-4986

[42] S. Chaudhuri, J. Gao, and K. Irwin, "Simulation and analysis of superconducting traveling-wave parametric amplifiers," *IEEE Transactions on Applied Superconductivity*, vol. 25, no. 3, pp. 1–5, 2015.

[43] D. E. McCumber, "Effect of ac impedance on dc voltage-current characteristics of superconductor weak-link junctions," *Journal of Applied Physics*, vol. 39, no. 7, pp. 3113–3118, 1968. [Online]. Available: https://doi.org/10.1063/1.1656743

[44] R. M. Biernacki, M. Marcu, and D. E. Root, "Circuit optimization with x-parameter models," in *2017 IEEE MTT-S International Microwave Symposium (IMS)*, 2017, pp. 1498–1500.

[45] S. A. Maas, *Nonlinear microwave and RF circuits*. Artech house, 2003.

[46] D. E. Root, J. Verspecht, J. Horn, and M. Marcu, *X-Parameters: Characterization, Modeling, and Design of Nonlinear RF and Microwave Components*. Cambridge University Press, 2013.

[47] C. M. Caves, "Quantum limits on noise in linear amplifiers," *Phys. Rev. D*, vol. 26, pp. 1817–1839, Oct 1982. [Online]. Available: https://link.aps.org/doi/10.1103/PhysRevD.26.1817

[48] A. Roy and M. H. Devoret, "Introduction to parametric amplification of quantum signals with josephson circuits," *Comptes Rendus Physique*, vol. 17, no. 7, pp. 740–755, 2016. [Online]. Available: https://www.sciencedirect.com/science/article/pii/S1631070516300640

[49] J. M. Manley and H. E. Rowe, "Some general properties of nonlinear elements-part i. general energy relations," *Proceedings of the IRE*, vol. 44, no. 7, pp. 904–913, 1956.

[50] H. A. Haus and J. A. Mullen, "Quantum noise in linear amplifiers," *Phys. Rev.*, vol. 128, pp. 2407–2413, Dec 1962. [Online]. Available: https://link.aps.org/doi/10.1103/PhysRev.128.2407

[51] A. A. Clerk, M. H. Devoret, S. M. Girvin, F. Marquardt, and R. J. Schoelkopf, "Introduction to quantum noise, measurement, and amplification," *Rev. Mod. Phys.*, vol. 82, pp. 1155–1208, Apr 2010. [Online]. Available: https://link.aps.org/doi/10.1103/RevModPhys.82.1155

[52] N. Bergeal, R. Vijay, V. E. Manucharyan, I. Siddiqi, R. J. Schoelkopf, S. M. Girvin, and M. H. Devoret, "Analog information processing at the quantum limit with a Josephson ring modulator," *Nat. Phys.*, vol. 6, no. 4, pp. 296–302, Apr. 2010.

[53] R. Kubo, "The fluctuation-dissipation theorem," *Reports on Progress in Physics*, vol. 29, no. 1, pp. 255–284, jan 1966. [Online]. Available: https://doi.org/10.1088/0034-4885/29/1/306

[54] V. Rizzoli, F. Mastri, and D. Masotti, "General noise analysis of nonlinear microwave circuits by the piecewise harmonic-balance technique," *IEEE Transactions on Microwave Theory and Techniques*, vol. 42, no. 5, pp. 807–819, 1994.

[55] E. Ngoya, "On the cyclostationary noise analysis in large rf integrated circuits," *IEEE Transactions on Circuits and Systems I: Regular Papers*, vol. 58, no. 11, pp. 2729–2740, 2011.

[56] S. Whiteley, "Josephson junctions in spice3," *IEEE Transactions on Magnetics*, vol. 27, no. 2, pp. 2902–2905, 1991.

[57] H. W. Bode *et al.*, "Network analysis and feedback amplifier design,"
1945.

[58] R. Fano, "Theoretical limitations on the broadband matching of
arbitrary impedances," *Journal of the Franklin Institute*, vol. 249, no. 1,
pp. 57–83, 1950. [Online]. Available: https://www.sciencedirect.com/
science/article/pii/0016003250900068

[59] Kylemark, Sunnerud, Karlsson, and Andrekson, "Semi-analytic satura-
tion theory of fiber optical parametric amplifiers," *Journal of Lightwave
Technology*, vol. 24, no. 9, pp. 3471–3479, 2006.

[60] J. C. Pedro, D. E. Root, J. Xu, and L. C. Nunes, *Nonlinear Circuit
Simulation and Modeling: Fundamentals for Microwave Design*, ser.
The Cambridge RF and Microwave Engineering Series. Cambridge
University Press, 2018.